JOURNAL OF Applied Polymer SCIENCE

The self-healing mechanism of an industrial acrylic elastomer

Fan Fan, Jerzy Szpunar
Department of Mechanical Engineering, College of Engineering, University of Saskatchewan, Saskatoon, Saskatchewan S7N 5A9, Canada
Correspondence to: F. Fan (E-mail: mike.fan@usask.ca)

ABSTRACT: The self-healing materials attract a lot of attention as self-healing ability considerably improves reliability of service and extends the life time of materials. However, the present self-healing materials lack the mechanical strength and thus cannot be used in practical applications. The industrial elastomer (VHB 4910) is a strong polymer, which has been used as dielectric actuator. Surprisingly, we observed that VHB 4910 has autonomic self-healing ability. As this is an acrylic polymer, we analyzed the hydrogen bonding between carbonyl and hydroxyl groups and demonstrated that this bonding and the molecular chain entanglement contributes to its self-healing ability. The tensile test, X-ray diffraction (XRD), Raman, and Fourier transform infrared (FTIR) spectroscopy were employed to analyze the self-healing processes. This study provides an insight into the mechanism of self-healing behavior and ability of VHB 4910 to recover its strength. © 2015 Wiley Periodicals, Inc. J. Appl. Polym. Sci. **2015**, *132*, 42135.

KEYWORDS: amorphous; elastomers; mechanical properties; rubber; thermosets

Received 15 December 2014; accepted 23 February 2015
DOI: 10.1002/app.42135

INTRODUCTION

Self-healing is an intrinsic property of biological systems such as human skin, which can heal the wound after injury. To elongate the life time of industrial products, researchers have created various self-healing materials. In 2002, White *et al.*[1] achieved a breakthrough by incorporating microcapsules, which contain a healing agent. When the crack nucleates and propagates, the microcapsules will be ruptured and release the healing agent to heal the crack by a polymerization process. However, this self-healing process cannot be repeated multiple times as the healing agent would be depleted. The polymers with reversible covalent bonds were developed to solve this problem; however, the requirements of external intervention such as heating and ultraviolet stimuli limits theirs application.[2–5] In 2008, Leibler *et al.* created a rubber-like material, which exhibited autonomic self-healing ability.[6] This supramolecular polymer was made of fatty acids and urea, which healed by hydrogen bonding. Their works initiated the application of noncovalent bonds to manufacture novel self-healing materials.

The autonomic self-healing materials have been applied in various laboratory type applications for developing novel biological materials,[7,8] coatings,[9,10] electronic skin,[11] and batteries.[12] The self-healing ability of these materials is attributed to the reversible noncovalent interactions in particular such as hydrogen bonding,[6,8,13–15] hydrophobic association,[16–20] ionic bonds,[21–24] and π-π stacks.[25,26] However, the low mechanical strength has limited the practical application of these materials.[27] To our surprise, we accidentally observed that the widely used and studied elastomer (VHB 4910) exhibits excellent autonomic self-healing ability. This elastomer can heal the cutting damage in the ambient environment without external intervention. Furthermore, the elastomer shows an excellent mechanical property as its toughness reaches up to ~1.91 MJ/m^3. The elastomer was previously used as dielectric actuator because of its electro-active properties.[28,29] Some of its viscoelastic properties have been studied by Steinmann and coworkers.[30] As this is acrylic polymer, we hypothesize that the hydrogen bonding between carbonyl bonds and hydroxyl groups and the molecular chain entanglement contribute jointly to its self-healing ability.[15]

To evaluate its self-healing behavior, we performed tensile tests on specimens of this material. The X-ray diffraction (XRD) pattern of VHB 4910 identified its amorphous structure. The Raman and Fourier transform infrared (FTIR) spectra illustrate its possible constituents and self-healing mechanism. In addition, the reptation model will be used to confirm the molecular chain diffusion at the cut interfaces.[31–34] To our best knowledge, it's the first study about the self-healing mechanism of VHB 4910. This study points out that this commercial product has the potential to be used for novel applications, such as coatings, where the self-healing ability is required.

EXPERIMENTAL

Materials and Sample Preparation

VHB 4910 was used as purchased from 3M Company with a cross section dimension of 25.4 × 0.889 mm^2. The main

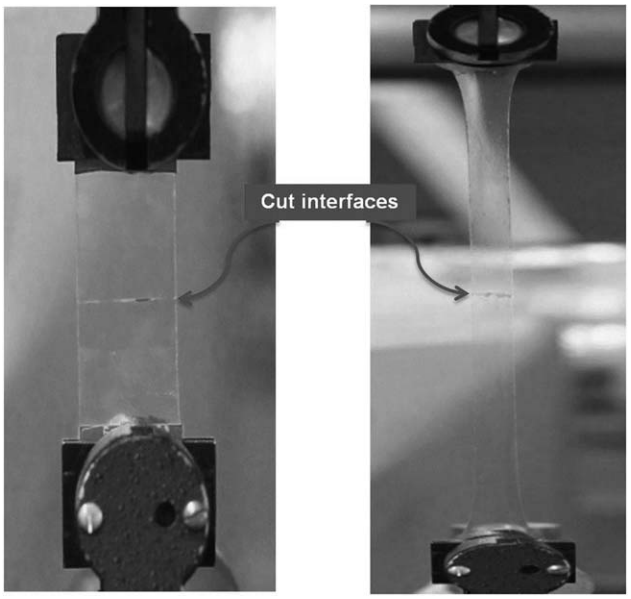

Figure 1. The tensile test of a healed sample confirmed that VHB 4910 has autonomic self-healing ability.

constituents of this material are acrylic but no detailed structural composition is known. The samples were cut into a rectangular shape with a length of 100 mm.

Fourier Transform Infrared Spectrum Measurements

The Fourier transform infrared (FTIR) spectra were scanned under room temperature with the IlluminatIR II inVia Reflex (Smiths Detection) equipped with a 36× ATR objective. The scanning range covered the wavenumbers from 650 to 4000 cm-1 with a resolution of 4 cm^{-1}.

Raman Spectrum Measurements

The Raman spectra were obtained using a Renishaw 2000 Raman Microscope. The wavelength of the laser source was 785 nm and the scattered light was dispersed with a grating of 1200 L/mm. The scattered laser light was collected by the Renishaw CCD camera. A 50× objective was chosen. The exposure time was set to 10 s with 1 accumulation. The laser power was 0.01 W. The glass slide was covered with an aluminum foil to remove the disturbance from silicon oxide. The sample was placed on the foil covered glass slide.

Uniaxial Tensile Tests

The uniaxial tensile tests were done with the INSTRON 3366 tensile machine with a 1 kN load cell. The sample length between two jaws is 50 mm. The cross speed was controlled at 100 mm/min. The samples were cut in the middle with a scalpel and brought into together with a slight force before the tensile tests.

RESULTS AND DISCUSSION

Mechanical Characterization of Self-Healing Behavior

This material shows autonomic self-healing ability in an ambient environment. The samples were separated into two pieces by a cut using a medical scalpel and then the cut pieces were brought into contact with a slight press. After healing periods from 10 to 960 min, the samples were stretched using a tensile machine at a constant speed of 100 mm/min (Figure 1). The samples can be stretched to a different strain depending on the healing time. Figure 2(a) shows that both the nominal fracture strain and stress increased with the healing time and respectively reached a value of ~727% and ~0.30 MPa after 240 min. The nominal fracture strain and stress leveled off after that and finally reached ~760% and ~0.35 MPa after a healing time of 960 min. This can be compared to the nominal fracture strain and stress of the original samples (~900% and 0.56 MPa).

The area under the strain-stress curve is defined as toughness and measures the work done by the tensile machine during the loading process. The material is very tough as its toughness is ~1.91 MJ/m^3, which is almost twice of the value (~1 MJ/m^3) that was obtained for the copolymer of acrylamide and acrylate.[17] The healing efficiency of the material is determined by the ratio of the toughness of the healed sample to that of the original sample.[22] Figure 2(b) shows that the self-healing efficiency increased with healing time and reached an average value of ~60% after a healing time of 240 min. In a relatively short healing time, the toughness of healed samples recovered to ~1.32 MJ/m^3, which is much higher than observed for other self-healing materials.[19,22] Moreover, the best healed sample

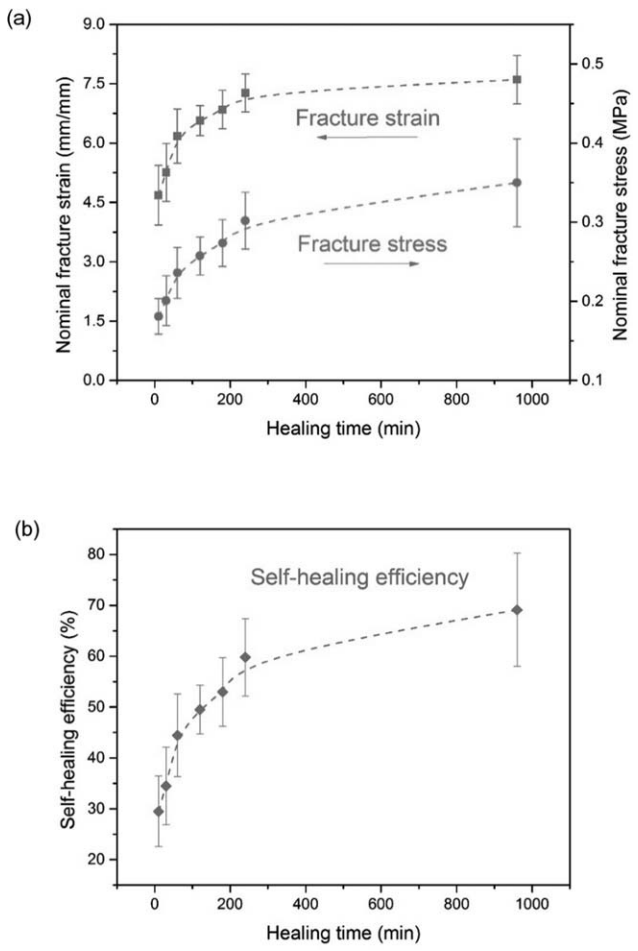

Figure 2. (a) The nominal fracture strain and stress of the healed samples in relation to the healing time from 10 to 960 min. (b) The self-healing efficiency changes as a function of the healing time from 10 to 960 min.

after 960 min at room temperature reached ~84% of the nominal tensile strength of the original samples [Figure 3(a)]. Its fracture stress and strain is respectively about 0.43 MPa and ~850%, which is rather close to 0.56 MPa and ~900% of the original samples. The deviation from the average value exists mainly because this material is notch sensitive and we cannot ensure that the contact of the cut specimens is perfect and small notches may nucleate the early failure.

Furthermore, we tested the influence of waiting time on the self-healing ability. The waiting time describes the period between cutting and contacting the samples. The cutting interfaces were expected to approach an equilibrium state after which the ability of self-healing is lost.[6] However, this materials exhibit an impressive self-healing ability even after a waiting time of 40 h. Figure 3(b) shows that after the same healing time of 120 min, the fracture strain and stress of the healed samples with a waiting time of 40 h only decreased by ~11% in comparison to the samples that were joined just after they were cut and separated.

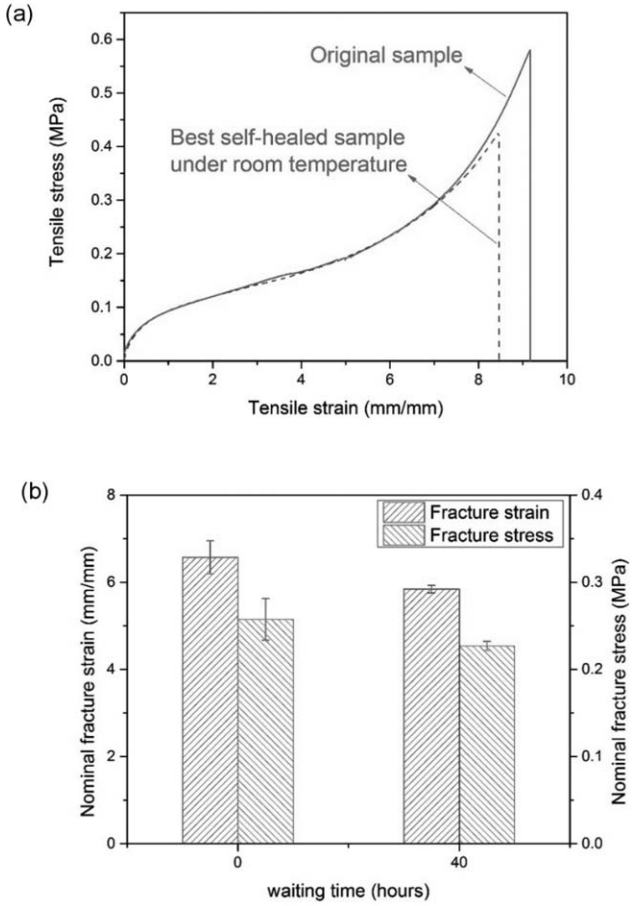

Figure 3. (a) The comparison of the strain–stress curve of the best healed sample after a healing time of 960 min under room temperature to the original sample. (b) The comparison of the mechanical strength of healed samples without or with a waiting time of 40 h.

The Role of Hydrogen Bonding in Self-Healing

Because possible constituents of our material are acrylate and acrylic acid, we assume that the self-healing can be realized by two mechanisms: reconstruction of hydrogen bonding and interdiffusion of the molecular chains.[15] Figure 4(a) shows the schematic process of the self-healing process between the cut interfaces. The (XRD) pattern demonstrated the amorphous structure of VHB 4910 [Figure 4(b)] and such structure provides random associations of the mobile chains and thus can generate rather diverse distribution of hydrogen bonds. Raman and FTIR spectroscopies of our samples allowed determination of the possible constituents of chemical bonds and the damage of chemical bonding. We compared Raman and FTIR spectra of our materials [Figure 4(c)] and the assignment of the bands is presented in Table I. The vibration frequency of carbonyl bonds (C═O) was recorded at 1707 and 1731 cm^{-1},[35] the hydroxyl group (—OH) deformation is at 1376 cm^{-1},[8] and the stretching of carbon oxygen bond (C—O) coupled with —OH in plane bending appears at a frequency of 1160–1255 cm^{-1} in the FTIR spectrum.[35,36] The results obtained confirm the existence of functional groups constituting poly(acrylic acid) in the investigated material.

As the carbonyl bond is likely responsible for hydrogen bonding with the hydrogen atom of hydroxyl groups, we focus the observation on the Raman spectrum from 1665 to 1780 cm^{-1} covering the possible range of carbonyl bonds. We scanned along a line which is 14 μm long and starts from the cut interfaces to the area that is not affected by the cut. Figure 5(a) illustrates the variation of the Raman spectra. The intensity increased continuously with the distance from the cut. This can be attributed to the smaller damage of chemical bonds at positions that are at larger distance from the cut. The second derivative plot of the Raman spectra indicates that there are two peaks in the carbonyl bands [Figure 5(b)]. The peak at the higher wavenumber represents the free carbonyl bonds while the other at a lower wavenumber is associated with the hydrogen-bonded carbonyl bonds.[35] Fitting by Lorentz function was applied to the Raman spectra in order to separate these two peaks [Figure 5(c)]. The results obtained close to the cut show two peaks at ~1670 and 1730 cm^{-1}. The band wavenumber of the hydrogen-bonded carbonyl bonds increased with the distance at first, but is leveled off at the distance of 2 μm, while the full width at half maximum (FWHM) decreased with the distance at first but also leveled after 2 μm [Figure 6(a)]. The hydrogen bonding constrains the vibration of original carbonyl bonds and thus the wavenumber decreases and the FWHM of the corresponding chemical bonds broadens.[35] The result confirms that there exists strong hydrogen bonding at the cut interface, which reassociates both parts. Compared with the hydrogen-bonded carbonyl bond, the band wavenumber and FWHM of the free carbonyl bond remained almost constant with the distance [Figure 6(b)]. In addition, the damage of the cut brought a stress field around the cut interfaces. The cut damage and the stress filed reduced both of the hydrogen bonded carbonyl bonds and the free carbonyl bonds. Figure 6(c) shows that both of the Raman intensities of the hydrogen bonded and the free carbonyl bonds decreased with the distance closer to the cut interfaces. However, the intensity ratio of the hydrogen bonded carbonyl bonds to the free carbonyl bonds increased when the distance is closer to the cut interfaces. This increasing ratio confirms that some

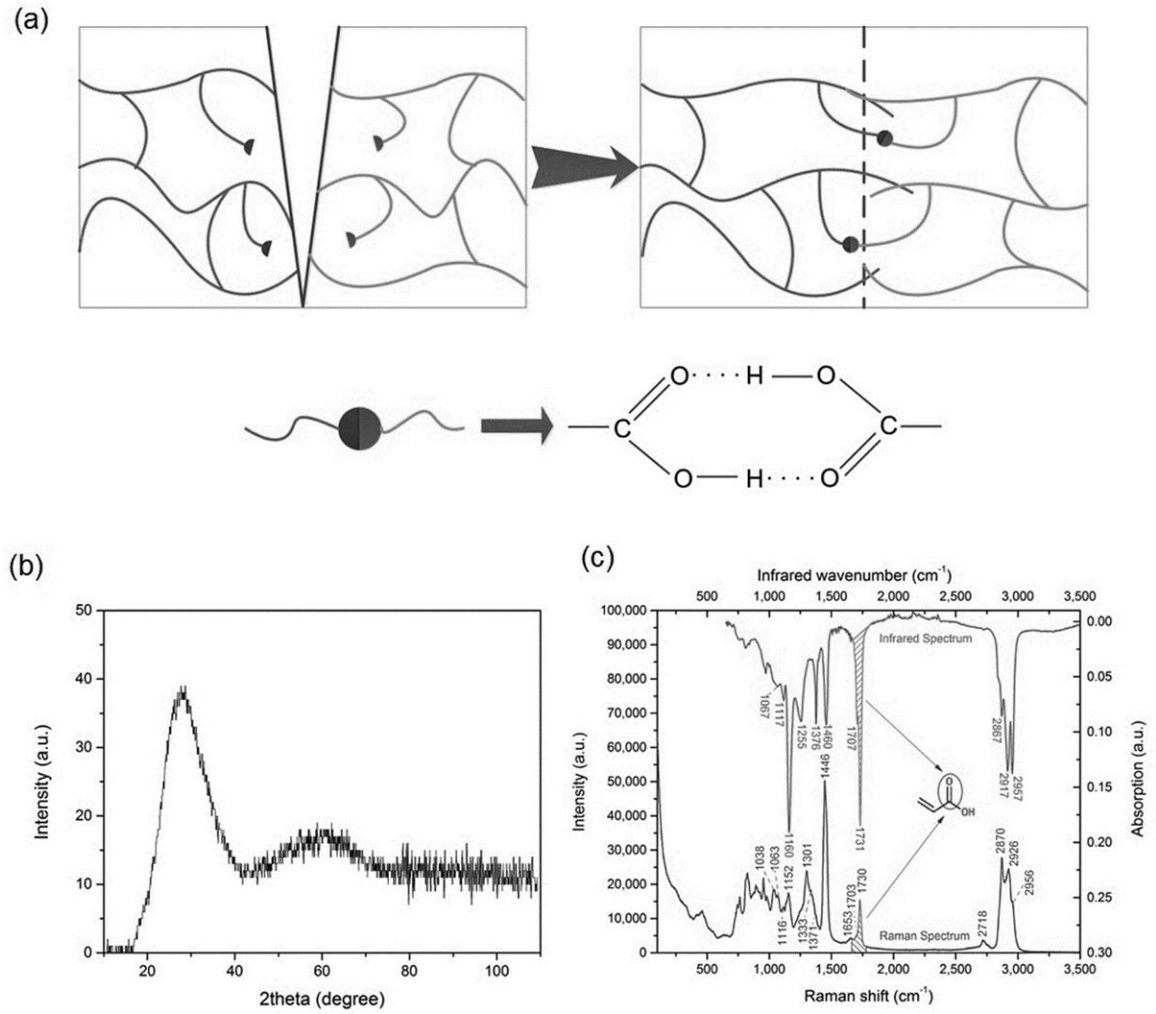

Figure 4. (a) The schematic healing process of VHB 4910 between the cut interfaces. (b) XRD shows that VHB 4910 is an amorphous material. (c) The peaks of Raman and FTIR were identified and the two peaks for carbonyl bonds were highlighted.

Table I. Observed Wavenumbers and Assignment of Raman and FTIR Bands

Raman (cm^{-1})	Infrared (cm^{-1})	Assignment
2956	2954	C—H3 stretching vibration[36]
2926	2917	C—H2 stretching vibration[36]
2870	2869	C—H2 stretching vibration[36]
2718		Overtone of 1446
1730	1731	C=O stretching vibration (free carboxylic)[35]
1703	1707	C=O stretching vibration (hydrogen bonded carboxylic)[35]
1663		Overtone and combination
1446	1459	CH2 scissors deformation or CH3 asymmetrical deformation[36]
1373	1376	OH deformation[8]
1333		CH2 twisting[35]
1301		CH2 wag or twisting[8]
	1255	C—O stretching coupled with O—H in-plane bending[35]
1152	1160	C—O stretching coupled with O—H in-plane bending[35,36]
1116	1117	C—CH2 stretching vibration[35]
1063	1067	C—O stretching vibrations[36]
1039	1037	CH2 rocking[35]

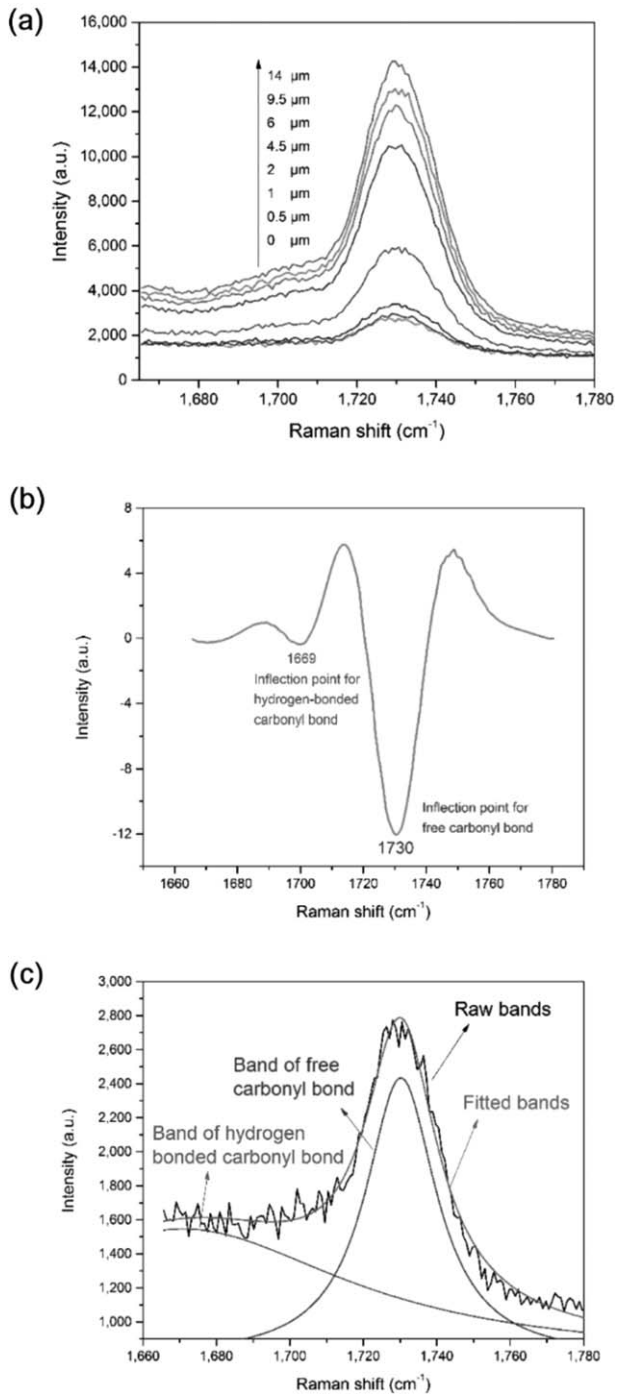

Figure 5. (a) The variation of the Raman spectra of carbonyl bonds along a scanning line, which is of 14 μm in length and perpendicular to the direction of the cut. (b) Second derivative plot of the Raman spectrum for a point close to the cut interfaces. (c) The curve fitting of the Raman spectra for a point at the cut interfaces.

free carbonyl bonds transferred to the hydrogen bonded carbonyl bonds at the cut interfaces.

To confirm that the hydrogen bonding contributes to the self-healing process, we made tensile tests on the urea immersed samples. As urea solution is known to be a chemical, which can disrupt hydrogen bonding,[37] we immersed the fresh cut interfaces into a 30 wt % urea solution for 1 min and then brought the interfaces into contact for 30 min. The fracture strain and stress of the urea-processed samples was reduced respectively to ~208% and ~0.11 MPa, both of which are half of the values obtained for the previously healed samples (Figure 7). Therefore, hydrogen bonding is verified to be one of the self-healing mechanisms of VHB 4910.

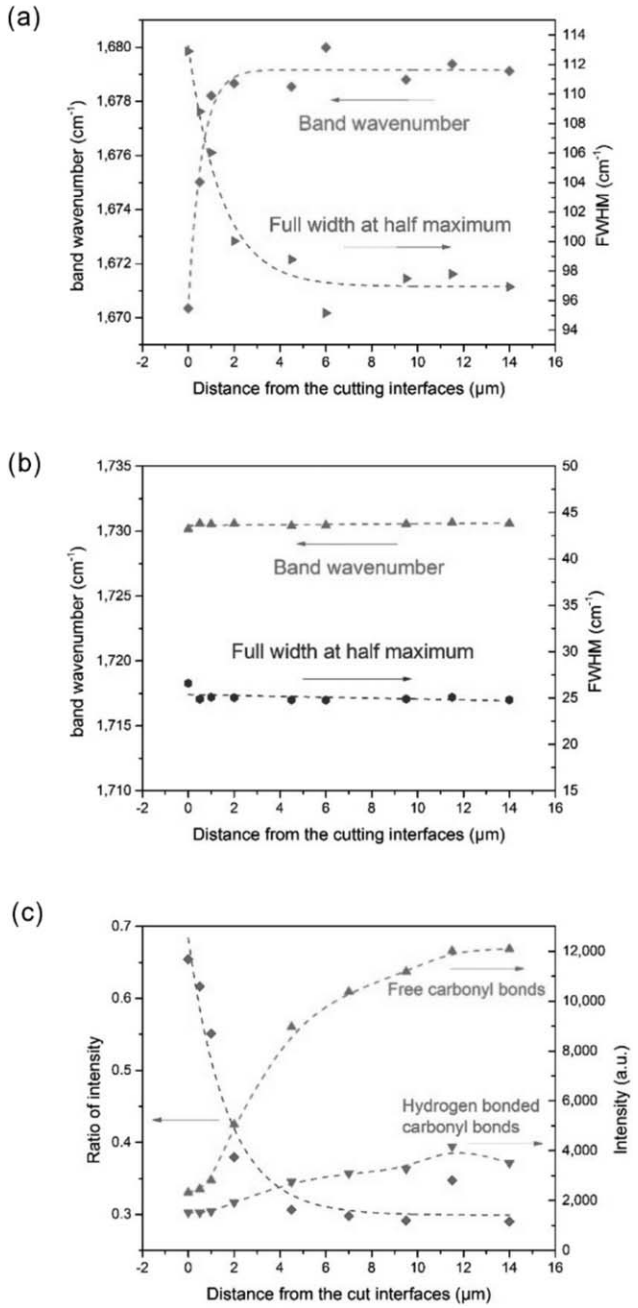

Figure 6. (a) The change of the band wavenumber and full width at half maximum (FWHM) for the hydrogen-bonded carbonyl bond at different distances from the cut interfaces. (b) The band wavenumber and FWHM for the free carbonyl bond remained almost constant with the distance to the cut interfaces. (c) The Raman intensities of two carbonyl bonds and the intensity ratio of the hydrogen bonded carbonyl bonds to the free carbonyl bonds change with the distance from the cut interfaces.

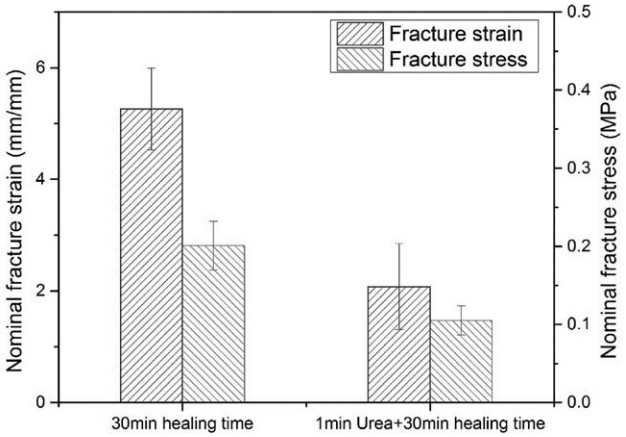

Figure 7. The influence of urea solution on the self-healing ability.

The Influence of Chain Diffusion on Self-Healing

According to Wool *et al.*,[33] the true fracture stress of healed samples (σ_{tr}) is proportional to $t^{0.25}$, where t is the healing time. Therefore, we can derive the relation between the true fracture stress and the healing time as:

$$\log_{10}^{\sigma_{tr}} = C + 0.25\log_{10}^{t} \quad (1)$$

where C is a constant decided by the material. As this material is an elastomer, the volume change during tensile tests was ignored.[38] Therefore, the true fracture stress σ_{tr} was calculated from:

$$\sigma_{tr} = \lambda \times F / A_{in} \quad (2)$$

where λ is the deformation ratio (deformed length/initial length), F is the force, and A_{in} is the initial cross-section area. Figure 8 shows that the relationship between the true fracture stress of the healed samples and the healing time in double-logarithmic coordinates. We fitted the data with a general linear equation and extracted the slope to be 0.25 with a standard deviation of 0.017. Such an agreement indicates that the chain diffusion process contributes to the self-healing and explains the time-dependence of the healing process.

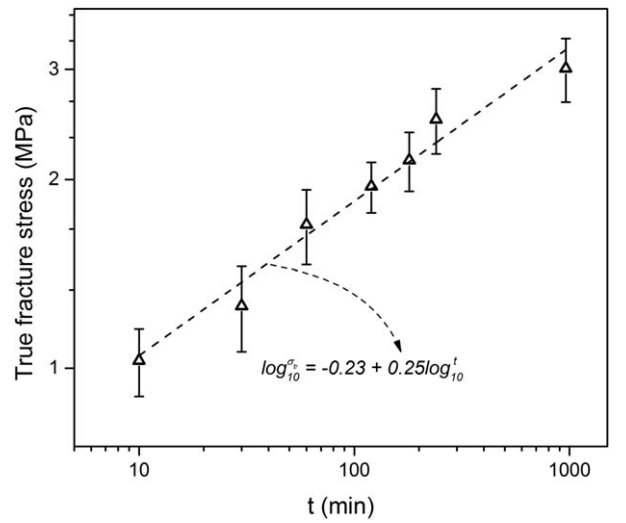

Figure 8. The proportional relationship between the true fracture stress of healed samples and the healing time in double-logarithmic coordinates.

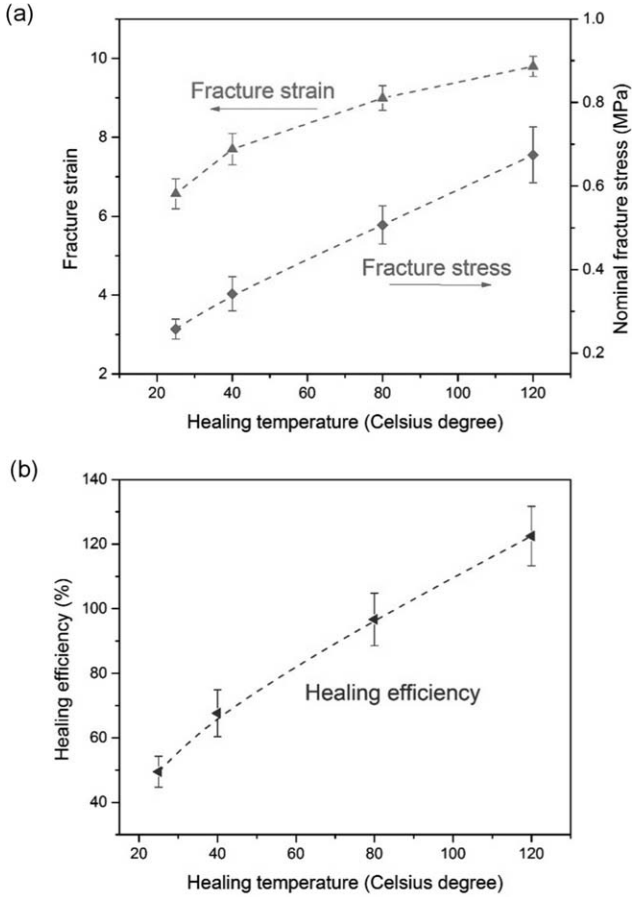

Figure 9. (a) Both of the fracture strain and stress increases with healing temperatures from 25 to 120°C for the same healing time of 120 min. (b) The healing efficiency increases healing temperature from 25 to 120°C under the same healing time of 120 min and reaches to more than 100% at 120°C.

Furthermore, the Flory's theory indicates that the mobility of molecular chains increases with the temperature.[34] We tested the healing ability of this material under different healing temperatures from 25 to 120°C with a same healing time of 120 min. Figure 9(a) shows that the fracture strain increases with the healing temperature and the fracture stress shows almost a proportional relation to the healing temperature. After healing at 120°C for 120 min, the fracture strain and stress of the healed samples recovered to ~980% and 0.67 MPa which are higher than the values measured for original samples (~900% and 0.56 MPa). As a result, the healing efficiency increased and reached ~123% at the healing temperature of 120 C [Figure 9(b)]. This significant improvement of self-healing ability can be attributed to the high temperature, which injects more energy into the healing process and promotes the chain entanglement at the cut interface.

We also scanned Raman spectra at two points on the sample that is healed for different healing times. One of the points is close to the line of cut while another is 30 μm from this line. Figure

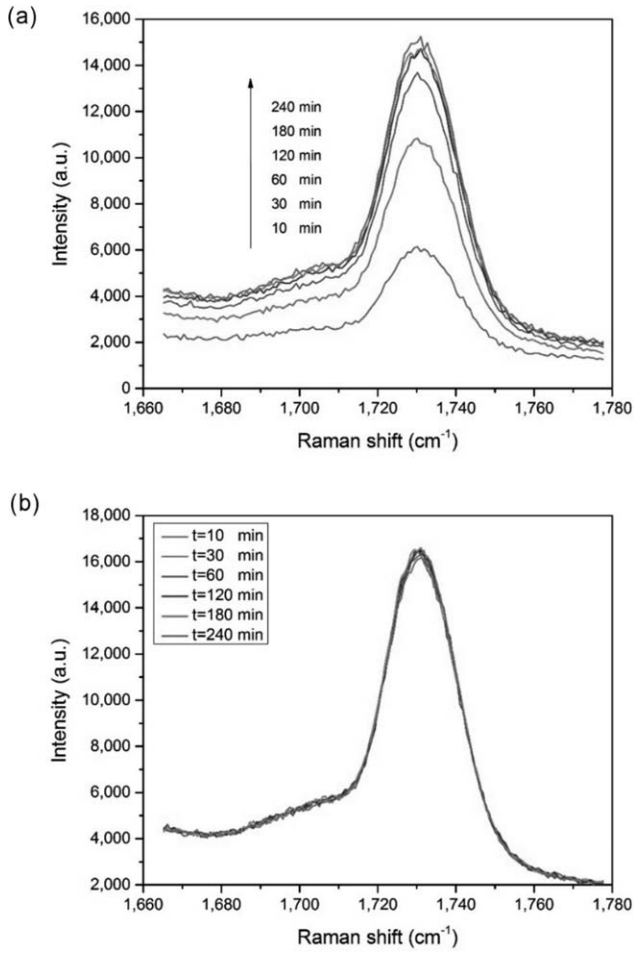

Figure 10. (a) The comparison of carbonyl bonds' intensities of Raman spectra with different healing times from 10 to 240 min for a point close to the cut interfaces. (b) The comparison of carbonyl bonds' intensities of Raman spectra with different healing times from 10 to 240 min for a point on the original surface.

10(a) shows that the intensity of the spectra for the point close to the cut increases with the time of healing. This behavior may be attributed to the chain diffusion, which facilitated molecular chains crossing the cut interfaces. With the increase of time, more molecular chains entangled and more hydrogen bonds reassociate. The entanglement and reassociation leads to the decrease of the chains mobility.[39] Therefore, the intensity increased significantly during the first 120 min, while the increase after that time is negligible. On the contrary, the spectra of the point on the original surface did not change much as it is too far to be affected by the chain diffusion process [Figure 10(b)].

CONCLUSIONS

We evaluated the self-healing ability of VHB 4910 with tensile tests for different healing times. The self-healing ability increases with the healing time. We demonstrated that the hydrogen bonding is responsible for the healing process based on the results obtained using Raman and Fourier transform infrared spectroscopies. The increased self-healing efficiency at higher temperatures and increased intensity of Raman spectra observed for longer healing times provides support for important role of chain diffusion in the self-healing process. When the cut interfaces were brought together, the free carbonyl bonds were associated by the hydrogen bonding, which created a bridge for the diffusion process. The diffusion of the molecular chains leads to the entanglement of them which strengthened the self-healing ability. During the healing process, the hydrogen bonding connects the damaged surfaces and provides a bridge for chain diffusion across the cut interface. The chain diffusion process creates chain entanglements.

ACKNOWLEDGMENTS

This research was financially supported by Canadian Science and Engineering Research Council (NSERC). Fan Fan gratefully acknowledges the support of China Scholarship Council (CSC).

REFERENCES

1. White, S. R.; Sottos, N. R.; Geubelle, P. H.; Moore, J. S.; Kessler, M. R.; Sriram, S. R.; Brown, E. N.; Viswanathan, S. *Nature* **2001**, *409*, 794.
2. Chen, X.; Dam, M.; Ono, K.; Mal, A.; Shen, H.; Nutt, S. R.; Sheran, K.; Wudl, F. *Science* **2002**, *295*, 1698.
3. Kavitha, A. A.; Singha, N. K. *ACS Appl. Mater. Interfaces* **2009**, *1*, 1427.
4. Kavitha, A. A.; Singha, N. K. *Macromolecules* **2010**, *43*, 3193.
5. Ghosh, B.; Urban, M. *Science* **2009**, *323*, 1458.
6. Cordier, P.; Tournilhac, F.; Soulié-Ziakovic, C.; Leibler, L. *Nature* **2008**, *451*, 977.
7. Nakahata, M.; Takashima, Y.; Yamaguchi, H.; Harada, A. *Nat. Commun.* **2011**, *2*, 511.
8. Phadke, A.; Zhang, C.; Arman, B.; Hsu, C.-C.; Mashelkar, R. A; Lele, A. K.; Tauber, M. J.; Arya, G.; Varghese, S. *Proc. Natl. Acad. Sci. U S A* **2012**, *109*, 4383.
9. Li, Y.; Li, L.; Sun, J. *Angew. Chem.* **2010**, *122*, 6265.
10. Andreeva, D. V.; Fix, D.; Möhwald, H.; Shchukin, D. G. *Adv. Mater.* **2008**, *20*, 2789.
11. Tee, B. C.-K.; Wang, C.; Allen, R.; Bao, Z. *Nat. Nanotechnol.* **2012**, *7*, 825.
12. Wang, C.; Wu, H.; Chen, Z.; McDowell, M. T.; Cui, Y.; Bao, Z. *Nat. Chem.* **2013**, *5*, 1042.
13. Maes, F.; Montarnal, D.; Cantournet, S.; Tournilhac, F.; Corté, L.; Leibler, L. *Soft Matter* **2012**, *8*, 1681.
14. Cui, J.; del Campo, A. *Chem. Commun.* **2012**, *48*, 9302.
15. Gulyuz, U.; Okay, O. *Soft Matter* **2013**, *9*, 10287.
16. Tuncaboylu, D. C.; Sari, M.; Oppermann, W.; Okay, O. *Macromolecules* **2011**, *44*, 4997.
17. Tuncaboylu, D. C.; Argun, A.; Sahin, M.; Sari, M.; Okay, O. *Polymer* **2012**, *53*, 5513.
18. Haque, M. A.; Kurokawa, T.; Kamita, G.; Gong, J. P. *Macromolecules* **2011**, *44*, 8916.
19. Tuncaboylu, D. C.; Argun, A.; Algi, M. P.; Okay, O. *Polymer* **2013**, *54*, 6381.

20. Tuncaboylu, D. C.; Sahin, M.; Argun, A.; Oppermann, W.; Okay, O. *Macromolecules* **2012**, *45*, 1991.
21. Sun, T. L.; Kurokawa, T.; Kuroda, S.; Ihsan, A.; Bin; Akasaki, T.; Sato, K.; Nakajima, T.; Gong, J. P.; Haque, M. A. *Nat. Mater.* **2013**, *12*, 932.
22. Burnworth, M.; Tang, L.; Kumpfer, J. R.; Duncan, A. J.; Beyer, F. L.; Fiore, G. L.; Rowan, S. J.; Weder, C. *Nature* **2011**, *472*, 334.
23. Wang, Q.; Mynar, J. L.; Yoshida, M.; Lee, E.; Lee, M.; Okuro, K.; Kinbara, K.; Aida, T. *Nature* **2010**, *463*, 339.
24. Sun, J.-Y.; Zhao, X.; Illeperuma, W. R. K.; Chaudhuri, O.; Oh, K. H.; Mooney, D. J.; Vlassak, J. J.; Suo, Z. *Nature* **2012**, *489*, 133.
25. Xu, Y.; Wu, Q.; Sun, Y.; Bai, H.; Shi, G. *ACS Nano* **2010**, *4*, 7358.
26. Burattini, S.; Colquhoun, H. M.; Fox, J. D.; Friedmann, D.; Greenland, B. W.; Harris, P. J. F.; Hayes, W.; Mackay, M. E.; Rowan, S. J. *Chem. Commun.* **2009**, *44*, 6717.
27. Gong, J. P. *Soft Matter* **2010**, *6*, 2583.
28. Michel, S.; Chu, B. T. T.; Grimm, S.; Nüesch, F. A.; Borgschulte, A.; Opris, D. M. *J. Mater. Chem.* **2012**, *22*, 20736.
29. Liu, Y.; Gao, M.; Mei, S.; Han, Y.; Liu, J. *Appl. Phys. Lett.* **2013**, *103*, 064101.
30. Hossain, M.; Vu, D. K.; Steinmann, P. *Comput. Mater. Sci.* **2012**, *59*, 65.
31. De Gennes, P. G. *J. Chem. Phys.* **1971**, *55*, 572.
32. Klein, J. *Nature* **1978**, *271*, 143.
33. Kim, Y. H.; Wool, R. P. *Macromolecules* **1983**, *16*, 1115.
34. Flory, P. J. *Proc. R. Soc. A Math. Phys. Eng. Sci.* **1956**, *234*, 60.
35. Dong, J.; Ozaki, Y.; Nakashima, K. *Macromolecules* **1997**, *30*, 1111.
36. Colthup, N. B.; Daly, L. H.; Wiberley, S. E. Introduction to Infrared and Raman Spectroscopy; Academic Press: San Diego, **1990**, Chapter *13*, pp 387–481.
37. McQueen-Mason, S.; Cosgrove, D. J. *Proc. Natl. Acad. Sci. U S A* **1994**, *91*, 6574.
38. Strobl, G. The Physics of Polymers: Concepts for Understanding Their Structures and Behaviour; Springer: Heidelberg, **1997**, Chapter *9*, pp 357–414.
39. Yang, Y.; Urban, M. W. *Chem. Soc. Rev.* **2013**, *42*, 7446.